Electronic and magnetic properties of iron hydride under pressure: An experimental and computational study using x-ray absorption spectroscopy and x-ray magnetic circular dichroism at the Fe K edge

Nadejda Bouldi, Philippe Sainctavit, Amélie Juhin, Lucie Nataf, Francois Baudelet

Electronic and magnetic properties of iron hydride under pressure: An experimental and computational study using x-ray absorption spectroscopy and x-ray magnetic circular dichroism at the Fe *K* edge

Nadejda Bouldi,[1,2,*] Philippe Sainctavit,[1] Amélie Juhin,[1] Lucie Nataf,[2] and François Baudelet[2]
[1]*IMPMC, UMR7590, CNRS, Sorbonne université, IRD, MNHN, 4 place Jussieu, 75005 Paris, France*
[2]*Synchrotron SOLEIL, L'Orme des Merisiers, Saint-Aubin, 91192 Gif-sur-Yvette, France*

(Received 28 June 2018; published 31 August 2018)

The application of a 3.5 GPa pressure on Fe in a H_2 environment leads to the formation of iron hydride FeH. Using a combination of high pressure x-ray absorption spectroscopy (XAS) and x-ray magnetic circular dichroism (XMCD) at the Fe *K* edge, we have investigated the modification of electronic and magnetic properties induced (i) by the transition from bcc-Fe to dhcp (double hexagonal)-FeH under pressure and (ii) by the compression of FeH up to 28 GPa. XAS and XMCD spectra under pressure have been computed in bcc-Fe and dhcp-FeH within a monoelectronic framework. Our approach is based on a semirelativistic density-functional theory (DFT) calculation of the electron density in the presence of a core hole using plane waves and pseudopotentials. Our method has been successful to reproduce the experimental spectra and to interpret the magnetic and electronic structure of FeH. In addition, we have identified a transition around 28 GPa, which is a purely magnetic transition from a ferromagnetic state to a paramagnetic state.

DOI: 10.1103/PhysRevB.98.064430

I. INTRODUCTION

The study of iron and iron hydrides under pressure presents a strong geophysical interest. Iron is the main constituent of the Earth's core but, according to seismic models, the density of the core is lower than the density of pure iron by several percent. This density deficit is attributed to the dissolution of light elements such as silicon, sulfur, oxygen, hydrogen, and carbon [1]. Hydrogen has become one of the major candidates for the light elements in the Earth's core with the observation of its solubility in Fe under high pressure conditions [2].

Interest for the properties of transition metal hydrides has also grown because the absorption of hydrogen by metals or alloys is a promising solution to address the problem of hydrogen storage which is crucial to allow its use as fuel [3].

Iron hydride FeH can be synthesized by application of a 3.5 GPa pressure on Fe in a H_2 environment [4,5]. We have investigated the transition from bcc-Fe to FeH and the effect of pressure on FeH up to 28 GPa using a combination of x-ray absorption spectroscopy (XAS) and x-ray magnetic circular dichroism (XMCD) (which is the difference between the absorption of left and right circularly polarized x rays for materials with a net magnetic moment) [6]. XAS and XMCD provide element-specific information on the electronic structure or the magnetic structure of the sample. As XAS and XMCD are recorded simultaneously, it allows us to obtain the structural and magnetic properties at the very same pressure, which is a valuable advantage considering the difficulties to know precisely and to reproduce pressure conditions. Performing XAS and XMCD experiments with hard x rays is mandatory to probe samples at high pressure in diamond anvil cells. Nevertheless, unlike the $L_{2,3}$ absorption edges for which well-established magneto-optical sum rules [7–9] allow us to extract spin and orbital contributions to the magnetic moment from the integral of the spectra, the quantitative analysis of *K*-edge XMCD spectra is far from straightforward. The support of theoretical interpretations is crucial to understand the experimental results.

In the present work, XAS and XMCD spectra have been computed at the Fe *K* edge for bcc-Fe and dhcp-FeH and using an efficient first-principles semirelativistic approach which relies on density-functional theory (DFT) with plane waves and pseudopotentials [10]. We analyzed the different contributions to the calculated spectra. Calculations for a fictitious dhcp-Fe phase with no H atoms give valuable information on the effect of H atoms on the electronic structure of Fe and also on the physical content of XMCD at the *K* edge. We have also studied both numerically and experimentally the disappearance of magnetism in FeH at a pressure of approximately 28 GPa and we have been able to bring out the existence of a pressure-induced magnetic transition.

The article is organized as follows. The experimental and computational details, as well as the crystallographic structures used for the calculations, are described in Sec. II. Section III is dedicated to the presentation of the results. The formation of dhcp-FeH under pressure is studied. The good agreement obtained between calculations and experiments has allowed a detailed interpretation of the experimental spectra. The impact of H atoms on the electronic structure of the two different Fe sites in dhcp-FeH is then discussed. Finally, the experimental results obtained at higher pressures, up to the disappearance of XMCD, are presented, revealing the existence of a ferromagnetic to paramagnetic transition that is substantiated by calculations.

*n.bouldi@thphys.uni-heidelberg.de, presently at the Institute for Theoretical Physics, Heidelberg University, Philosophenweg 19, 69120 Heidelberg, Germany.

II. METHODOLOGY

A. Experimental details

A commercial polycrystalline iron foil (Fe, 99.99%) was placed into a membrane diamond anvil cell (DAC) [11] filled with dihydrogen gas (H_2) using a gas loader. In this experiment H_2 was both the pressure transmitting medium and a source of hydrogen. A small ruby was also loaded within the DAC to monitor the pressure inside the cell through the measurement of its fluorescence [12]. A Re gasket has been used. The pressure on the sample was varied from atmospheric pressure up to a pressure as large as 28 GPa. All the experiments were performed at room temperature.

Fe *K*-edge XAS and XMCD measurements were performed at the ODE beamline of synchrotron SOLEIL, which is a bending magnet beamline dedicated to dispersive XAS experiments [13]. The spectra were recorded in transmission mode with a Si(111) polychromator. The x-ray beam has been focused to a size of around $35 \times 35\ \mu m^2$ at the sample position. To obtain circular polarized x rays, a portion of the beam below the plane of the emitted radiation was selected and XMCD spectra were acquired by measuring the absorption cross section (XAS) under a 1.3 T magnetic field alternatively parallel and antiparallel to the propagation direction of the beam.

B. Computational method

First-principles calculations were performed using the suite electronic-structure calculations QUANTUM ESPRESSO [14] which is based on DFT using a plane-wave basis set, pseudopotentials, and periodic boundary conditions. The XAS and XMCD spectra are obtained in two steps: first, the electronic charge density is obtained self-consistently using the PWscf package, then spectra are computed using XSpectra [15,16] (which relies on a continued fraction approach based on projector augmented-wave reconstruction and the Lanczos algorithm). The two-dimensional (2D) and three-dimensional (3D) electron density depicted in Fig. 5 were obtained with the PP code from the result of the self-consistent calculation.

For the self-consistent calculation, Troullier-Martins [17] norm-conserving pseudopotentials were used with the formulation of Perdew-Burke-Ernzerhof [18] (GGA) for the exchange and correlation functional. The cutoff energy was set to 160 Ry. A Methfessel-Paxton cold smearing of 0.14 eV (0.01 Ry) was used. The size of the Γ-centered *k*-point grid needed to reach convergence of the spectra was determined to be $7 \times 7 \times 7$ for bcc-Fe and $12 \times 12 \times 4$ for dhcp-FeH using the conventional cells (respectively 2 and 4 Fe atoms per cell).

Spin-orbit coupling (that must be included to compute XMCD) is added as a perturbation to the DFT pseudo-Hamiltonian [19] within the diagonal spin-orbit coupling approximation with collinear spin along the [001] direction.

In the calculations in which results are presented in Figs. 2 and 3, a 1*s* core hole was added within the static approximation by removing a core electron in the pseudopotential of the absorbing Fe atom. A jellium background charge was added in order to ensure charge neutrality. A supercell was built to minimize the interactions between periodically reproduced core holes, and the *k*-point grid was reduced accordingly.

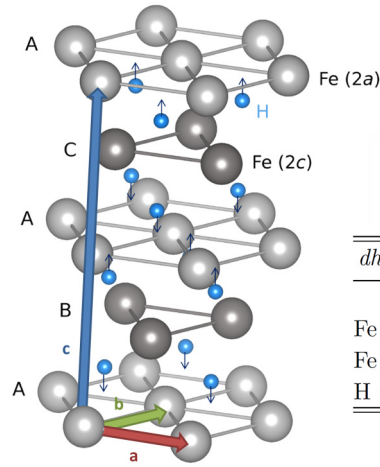

dhcp-FeH $P6_3/mmc$

		x	y	z
Fe (2*a*)	$\bar{3}$m	0	0	0
Fe (2*c*)	$\bar{6}$m2	1/3	2/3	1/4
H (4*f*)	3m	1/3	2/3	z_H

FIG. 1. Crystal structure of dhcp-FeH [25]. Iron atoms are shown in two different colors to emphasize the fact that they occupy nonequivalent sites. Letters A, B, and C are the usual notations for close-packed layers in compact structures. The atomic coordinates in the conventional unit cell (a, b, c) and the site symmetries are given in the table. If H atoms were positioned in the middle or the interlayer, $z_H = 0.875$. The experimental [25] value of z_H is 0.882, while in the present study z_H was determined to 0.880 from atomic relaxation. The arrows represent the direction of their displacement with respect to the middle of the interlayer.

In order to obtain the XAS and XMCD spectra, the relevant cross terms of the three operators from the semirelativistic cross section [10,20] were computed: electric dipole–electric dipole (D-D), electric quadrupole–electric quadrupole (Q-Q), and electric dipole–spin position (D-SP). The wave vector **k** was set along the axis [001]. A $20 \times 20 \times 20$ and a $27 \times 27 \times 9$ *k*-point grid were used for bcc-Fe and dhcp-FeH, respectively.

The spectra depicted in Figs. 2, 3, and 4 were convolved with a Lorentzian broadening function to simulate the effect of the finite lifetime of the 1*s* core hole (constant in energy, FWHM = 1.25 eV) and of the inelastic scattering of the photoelectron (additional energy-dependent broadening) for which we use the curve published for Fe by Müller *et al.* [21]. The spectra depicted in Fig. 8 were convolved with a Lorentzian of constant FWHM = 1.6 eV in order to see the miscellaneous peaks far from the edge in XMCD and measure the energy shifts. Experimental and calculated spectra were normalized such that the edge jump is equal to 1. During the calculation of the spectra the origin of the energy is set to the Fermi (E_F) energy of the material. A rigid shift in energy was then applied to the calculated spectra to make the maximum of the calculated XAS correspond to the maximum of the experimental spectrum. The same shift was applied to the XMCD spectrum.

Figure 1 was drawn with the help of VESTA [22] and Fig. 5 is drawn with XCrySDen [23].

C. Crystallographic structures

For bcc-Fe, the experimental lattice parameter [24] $a = 2.87$ Å is used. The supercell ($4 \times 4 \times 4$ unit cell) contains

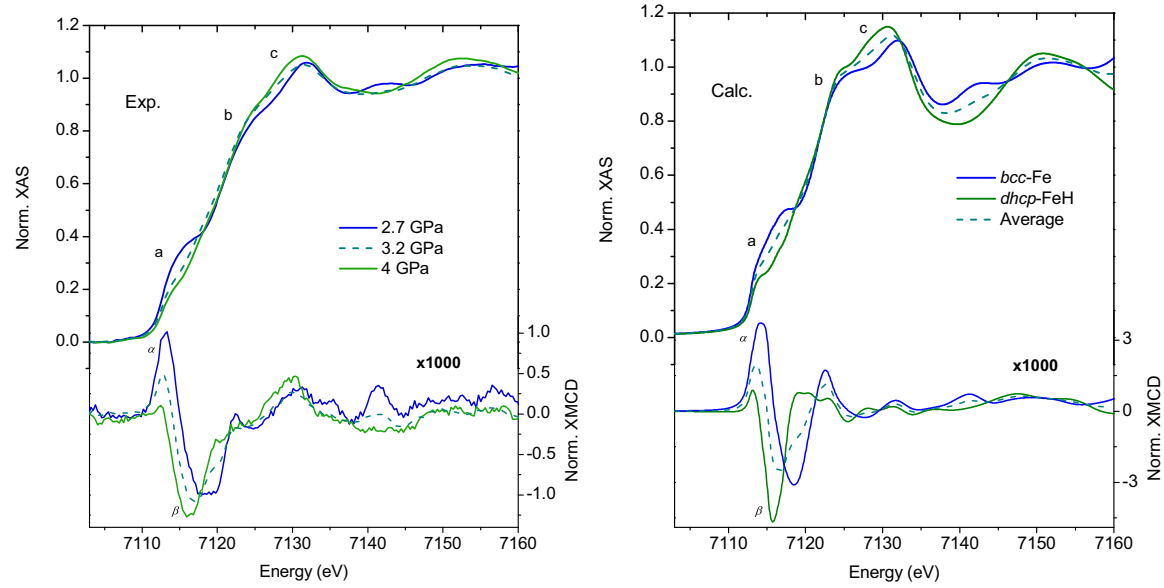

FIG. 2. Left: Experimental XAS and XMCD spectra at the Fe K edge of a Fe foil under H_2 atmosphere before (blue/dark gray solid), during (blue/gray dashed), and after (green/light gray solid) the pressure induced transition. Right: Calculated XAS and XMCD spectra at the Fe K edge in bcc-Fe (blue/dark gray solid) and dhcp-FeH (green/light gray solid). The dashed lines represent the average of the spectra for Fe and FeH. The experimental XMCD spectra were not corrected for the rate of circular polarization of the light $P_c \approx 0.7$.

64 atoms so the smallest distance between the periodically repeated core holes is 9.94 Å.

FeH has a double hexagonal closed pack lattice [5,25] (see Fig. 1). The stacking sequence of the Fe layers follows the pattern ABAC where A, B, and C are the usual letters to represent the three possible orientations of the layers.

The conventional cell contains four Fe atoms and four H atoms. There are two nonequivalent crystallographic sites which contain Fe atoms. The symmetry of one of these sites is trigonal [(2a): $\bar{3}$m] and the symmetry of the other site is hexagonal [(2c): $\bar{6}$m2]. H atoms are positioned in the interlayer. There is no symmetry constraint on the z coordinate of H atoms and, because of the low scattering cross section of H, it is not possible to determine the exact position of the H atoms using x-ray diffraction.

Neutron powder diffraction experiments performed on quenched FeD samples [25] showed that D atoms were

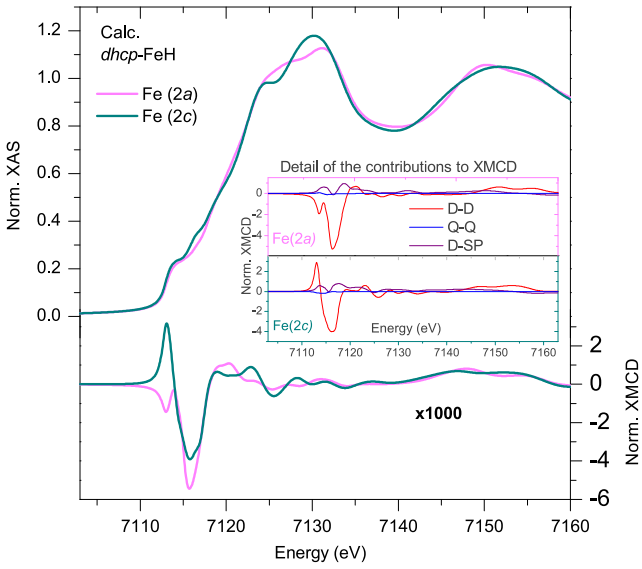

FIG. 3. Calculated contributions of the two crystallographic sites to the XAS and XMCD spectra at the K edge of Fe in dhcp-FeH (sum of the three terms D-D, Q-Q, and D-SP with the absorbing atom in one site or the other). Inset: Detail of the three terms of the cross section in the XMCD of each site.

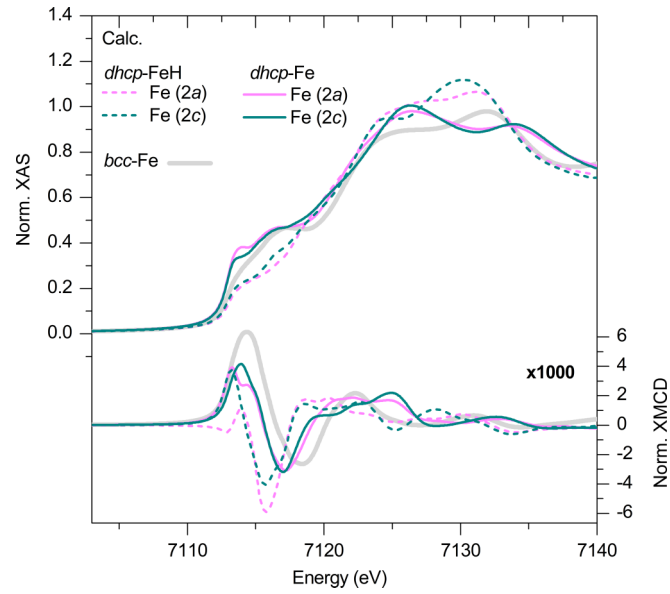

FIG. 4. Calculated contributions of both crystallographic sites to the XAS and XMCD spectra at the K edge of Fe in dhcp-Fe (solid lines) and dhcp-FeH (dashed lines) in the absence of core hole. In light gray, XAS and XMCD spectra in the absence of core hole in bcc-Fe.

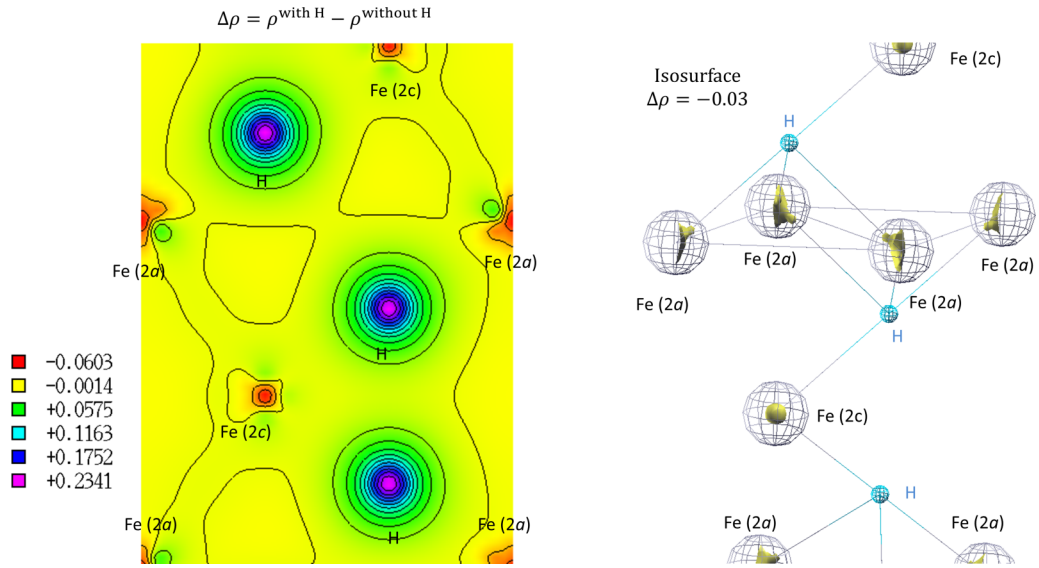

FIG. 5. Left: Difference between the electron density calculated for dhcp-FeH and dhcp-Fe in the [110] plane which contains both types of Fe atoms and H atoms. Only a portion of the cell is represented. Right: Isosurface $\Delta\rho = -0.03$ on the same portion of the cell. For this calculation, H atoms were positioned at the middle of the interlayer ($z_H = 0.875$).

positioned slightly off the center of the interlayer at $z_H = 0.882$. This vertical displacement was confirmed for FeH by DFT calculations [26]. In the present study we first performed an energy minimization by relaxing the atomic positions of H atoms and found $z_H = 0.880$, in good agreement with both experiment and previous calculations. For the sake of comparison, XAS and XMCD spectra were computed at Fe K edge for $z_H = 0.875$ (middle of the interlayer) and $z_H = 0.880$. The difference between the obtained spectra is so small that it almost lies within the linewidth when they are plotted.

To simulate the effect of pressure in the calculation, we decrease the lattice parameters of the crystal used for the numerical calculations. We use Vinet equation of states [27] with parameters [5] $V_0 = 55.6$ Å^3, $B_0 = 121$ GPa, and $B_0' = 5.31$ and we set the ratio c/a to the experimental value [25] 2×1.637. For example, for $P = 3$ GPa we use $a = 2.68$ Å and $c = 8.76$ Å.

III. RESULTS AND DISCUSSION

A. Transition from Fe to FeH under pressure

The measured XAS and XMCD spectra correspond to those of bcc-Fe for pressures between atmospheric pressure and 2.7 GPa and then they change significantly for larger pressures as illustrated in the left panel of Fig. 2. Consistently with previous experiments of the same kind [28], we observe a transition around 3 GPa. In XAS, the main changes near the edge are a decrease of the shoulder at 7115 eV (a) and a shift to lower energy ($\approx$1 eV) of the maximum c at 7131 eV accompanied by an enhancement of this maximum. In XMCD, the main positive peak α decreases in amplitude to become almost zero. The amplitude of the main negative peak β, on the other hand, increases and it becomes sharper. Peak β is also clearly shifted to lower energies (from 7118.5 eV at 2.7 GPa to 7116 eV at 4 GPa) while the energy position of peak α barely varies (from 7113 to 7112.5 eV).

When the pressure is decreased from 28 GPa to atmospheric pressure, the spectra corresponding to bcc-Fe are recovered between 4 and 2.5 GPa. In other words, the pressure-induced transition is reversible and the transition pressure is approximately the same whether the pressure is increased or whether it is decreased.

The pressure at which the changes are observed corresponds to the pressure of a transition reported in the literature [5,29,30] from Fe to iron hydride FeH. To confirm the nature of the transition, we performed calculations of the XAS and XMCD spectra of dhcp-FeH. At $P = 3$ GPa, the self-consistent calculation converges to a ferromagnetic structure with a total magnetization of 2.2 μB per Fe atom, which is consistent with the magnetometry experiments [4] while previous DFT calculations underestimated it to around 1.9 μB per Fe atom [26,31]. The calculated spectra, which are depicted in the right panel of Fig. 2 along with the spectra for bcc-Fe, are also in good agreement with the experiments, except for the amplitude of the XMCD signal which is not as fairly well described by our numerical method [10]. All the changes observed between the experimental spectra at $P < 2.7$ GPa and at $P > 4$ GPa are also observed between the calculated spectra for bcc-Fe and dhcp-FeH. This confirms that hydrogen can be absorbed into the iron lattice by application of pressure under an H_2 atmosphere, as was previously shown [4,5].

The experimental spectra acquired at the intermediate pressure 3.2 GPa are very similar to the calculated average of the calculated spectra for bcc-Fe and dhcp-FeH which is consistent with the fact that diffraction experiments [5] showed a coexistence of the two phases within the transition.

The XAS and XMCD spectra for dhcp-FeH shown in Fig. 2 are obtained numerically as the average of the spectra for each inequivalent Fe site. A significant advantage of performing calculations is the possibility to disentangle the contributions to the spectra from the different Fe atoms in the unit cell.

The calculated spectra are shown in Fig. 3. In the inset, the contributions to XMCD of the three terms of the semirelativistic cross section [20] are plotted. For both sites, the electric dipole–electric dipole term (D-D) dominates and the electric quadrupole–electric quadrupole term (Q-Q) is negligible. The electric dipole–spin position term (D-SP) is sizable though way smaller than the D-D term. In XAS, only the D-D term is significant.

The spectra for the two sites are very different. In particular the XMCD signal is mainly composed of two negative peaks for site ($2a$) and of a positive peak followed by a negative peak for the site ($2c$) so that the contribution from site ($2c$) seems more similar to the XMCD spectrum of bcc-Fe.

From partial density of states (DOS) projected on each atom, we can also obtain the contribution to the spin magnetization from a certain type of electron of a given atom. The spin magnetic moment due to the d electrons of Fe are slightly different for the two sites: $m_S^d = 2\langle S_z^d\rangle\mu_B = 2.21\,\mu_B$ for site ($2a$) and $m_S^d = 2.34\,\mu_B$ for site ($2b$). So, in accordance with Ref. [26], we find that Fe atoms closer to the H atoms have a smaller magnetic moment. Yet, it is not the cause of the difference between XMCD spectra. Indeed, when H atoms are positioned in the middle of the interlayer, the contribution of the Fe $3d$ electrons to the spin magnetic moment is the same for both sites ($2S_{z,d} = 2.28\,\mu_B$) but the calculated spectra remain almost unchanged. It is interesting to note that the integrals of both calculated XMCD spectra are very different [($2a$): -11×10^{-6}, ($2c$): -3×10^{-6} arb. unit]. This is a good illustration of the fact that the integral of the XMCD signal at the K edge is not proportional to $S_{z,d}$ (which is here the main contribution to the total magnetic moment).

We can get to a similar conclusion from the experimental XMCD spectra of bcc-Fe and dhcp-FeH whose integrals do not have the same order of magnitude (Fe: -6.5×10^{-4}, FeH: -6.6×10^{-3} arb. unit) even though the two materials have identical magnetic moments ($2.2\,\mu_B$ per Fe atom).

B. Effect of the absorption of H atoms on the electronic structure of Fe

The sum rules of XMCD at the K edge [7,9,10] for the electric dipole terms (D-D and D-SP) indicate that XMCD at the K edge probes the ground state expectation value of the spin and orbital operators restricted to the p electrons. The fact that XMCD spectra of bcc-Fe and dhcp-FeH are very different indicates that the fine magnetic structure around the Fe atoms is not similar in both compounds.

It is *a priori* difficult to predict if it is due to the structural modification from bcc to dchp or to the presence of H atoms. In dhcp-FeH, H atoms carry a weak spin magnetic moment in the opposite direction with respect to the moments on Fe atoms ($-0.03\,\mu_B$ per H atom). They almost do not contribute to the total magnetic moment in the cell. To better understand their effect on the magnetic structure of FeH, calculations were performed using a dhcp cell with Fe atoms at the same position as in dhcp-FeH but without H atoms. This phase, labeled dhcp-Fe phase, is purely fictitious because the presence of H atoms is required to stabilize the dhcp structure.

The self-consistent calculation for dhcp-Fe converges toward a ferromagnetic state with a total magnetic moment of $2.6\,\mu_B$ per Fe atom. The atoms are more distant from each other in dhcp-Fe (2.68 Å) than in bcc-Fe (2.49 Å). The fact that the magnetic moment is larger in dhcp-Fe is, therefore, consistent with the fact that the magnetic moment decreases when the interatomic distance is reduced, as done experimentally by application of pressure [32].

The contributions to the XAS and XMCD spectra at the Fe K edge from each Fe site in dhcp-Fe are depicted in Fig. 4 and compared with the spectra of dhcp-FeH and bcc-Fe for ease of comparison. The spectra of dhcp-Fe are visually more similar to the spectra of bcc-Fe than to those of dhcp-FeH. It shows that the change of the spectral features is only partially due to the transition from the bcc to the dhcp structure. In other words, H atoms, despite their weak magnetic moment, have a strong impact on the XMCD measured at the Fe K edge. Notably, in dhcp-Fe, the overall shape of the XMCD spectra is the same for both sites and, as the XMCD spectrum of bcc-Fe, it is composed of one positive peak followed by one negative peak.

The effect of H atoms on sites ($2a$) and ($2c$) is not the same: in the presence of H atoms (comparison of dashed and solid lines in Fig. 4) the main negative peak is shifted to lower energy and becomes sharper for both sites but for site ($2a$) the first positive peak disappears, whereas for site ($2c$) it retains almost the same amplitude.

To understand why there is such an asymmetry in the effect of hydrogen atoms on the XMCD of each site, we compared the electronic structure of dhcp-FeH with that of dhcp-Fe. The representations of the difference of the electron density of the two compounds in Fig. 5 show how the presence of H atoms in the interlayer affect the two sites. The left panel of Fig. 5 represents the difference $\Delta\rho$ of the electronic density between dhcp-FeH and dhcp-Fe on the crystallographic plane [110]. This plane was chosen because it contains Fe ($2a$), Fe ($2c$), and H atoms. Unsurprisingly, the main effect of adding H atoms in the interlayers is the increase of the probability of the presence of an electron at the position of the H atoms. The electron density near the Fe atoms is also modified: the electronic charge density around the Fe nucleus decreases due to the chemical bounding with the H atoms. On the right panel of Fig. 5, a 3D representation of the isosurface $\Delta\rho = -0.03$ is drawn. It is clearly visible that the electron density near site ($2a$) is affected differently by the presence of H atoms than the electron density near site ($2c$): near site ($2c$) the isosurface draws a sphere, whereas near site ($2a$) it draws lobes in the directions of the Fe-H bounds. It seems therefore that the substantial change of the shape of the XMCD spectrum of site ($2a$) when H atoms are added is related to an nonspherical redistribution of the electron density.

The changes observed between the XMCD spectra in bcc-Fe and dhcp-FeH are, therefore, markers of changes of the electron and spin distribution around the Fe atoms due both to the bcc to dhcp transition and to the presence of hydrogen atoms in the interlayer.

C. Compression of FeH and disappearance of magnetism

After the transition to FeH was achieved (above 4 GPa), the pressure on the sample was further increased in order to study the effect of pressure on iron hydride. Application of pressure

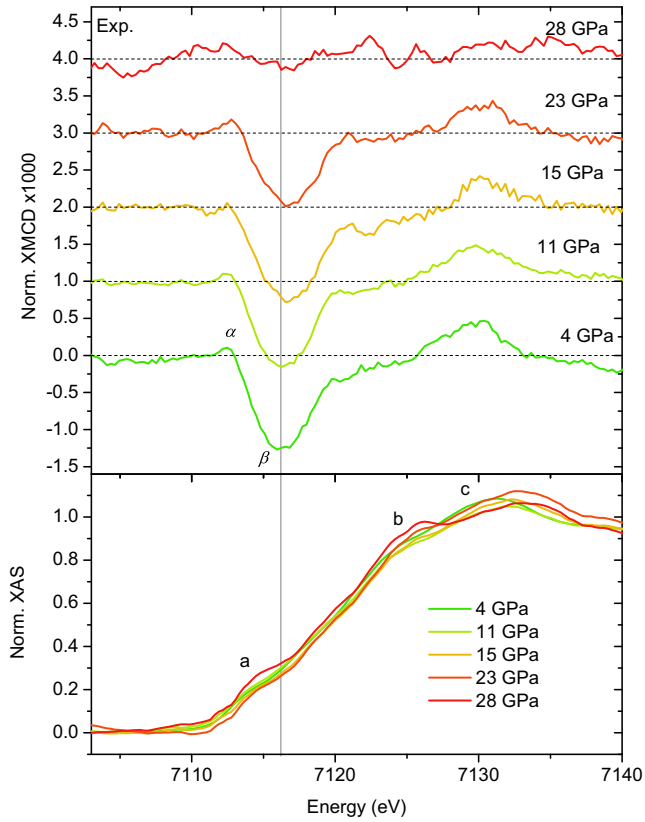

FIG. 6. Experimental XAS and XMCD spectra for FeH for several values of increasing pressure (the experimental XMCD spectra were not corrected for the circular polarization rate of the light $P_c \approx 0.7$).

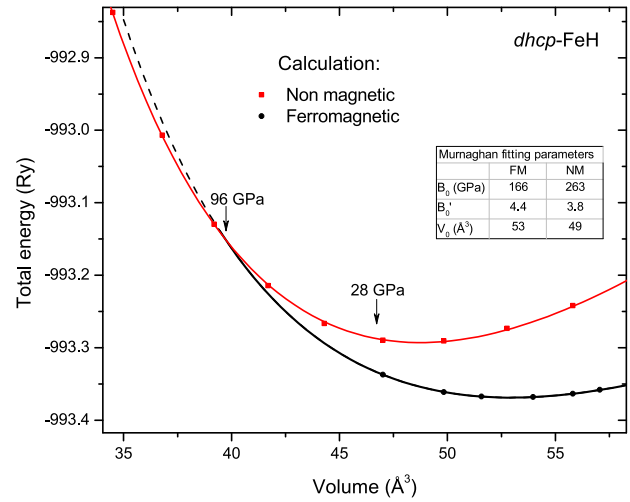

FIG. 7. Calculated total energy as a function of the volume of the dhcp-FeH cell. Red squares correspond to nonmagnetic (NM) calculations and black circles to spin-polarized calculations that converged into a ferromagnetic (FM) structure. Both curves are fitted with Murnaghan equation of state [36]. The fitted parameters are displayed in the table. The arrows indicate the pressure corresponding to the volume at their abscissa.

is a way of experimentally changing the interatomic distances which can lead to new properties of matter. Numerically, pressure is a test of the robustness of the method because it impacts the interaction strengths in the material.

Experimentally, the only change on the XAS spectrum between 4 and 23 GPa (see bottom panel of Fig. 6) is a progressive shift of the features to higher energies as the sample is compressed due to the reduction of distances: peak *c*, for example, is shifted by 1.6 eV between 4 and 23 GPa. The main effect of pressure on the XMCD spectrum (see top panel of Fig. 6) is a slight decrease in amplitude. The maximum of the effect is also progressively shifted to higher energies: peak β is shifted by 0.6 eV between 4 and 23 GPa.

XMCD vanishes between 23 and 28 GPa, which is consistent with the observation made by Mössbauer spectroscopy [33] and previous XMCD experiments [28] that magnetic ordering vanishes at pressures higher than approximately 27 GPa. The XAS spectrum also exhibits drastic changes at 28 GPa: the shoulders *a* and *b* are enhanced and the maximum *c* is reduced. In the literature, no change of the H content nor of the structure of the iron hydride was observed by XRD with compression up to 136 GPa of Fe under H_2 atmosphere (see Ref. [34] for the phase diagram of the Fe-H system).

To understand the disappearance of ferromagnetism under pressure in FeH, it is interesting to study the condition of stability of the ferromagnetic state compared to the paramagnetic state. The proper way of modeling a paramagnetic state would require a random distribution of localized magnetic moments (as it is done for example in Ref. [35] using SPR-KKR method) which is, to the best of our knowledge, computationally insurmountable with plane-waves DFT codes. It is therefore very common to describe paramagnetic states by states where all atoms have no net magnetic moments (i.e., for each atom, the density of spin up and spin down electrons are the same). The states obtained this way are usually referred to as *nonmagnetic states*. We will use this denomination in the following because it corresponds to the way the system is treated numerically.

The total energies of the nonmagnetic and ferromagnetic states of dhcp-FeH are plotted in Fig. 7 as a function of the volume of the double hexagonal cell. For volumes $V \leqslant 40$ Å^3, the nonmagnetic state becomes more stable which indicates that a ferromagnetic to paramagnetic transition happens. The present transition volume $V_t = 40$ Å^3 is close to the result obtained by LMTO-ASA calculations [31] that showed a magnetic transition between 75 and 80 bohr^3 (44–47 Å^3). The volume V_t corresponds experimentally to the pressure $P = 92$ GPa by application of the equation of state for FeH [5]. By applying the Murnagham equation of state to the calculated electronic structure, we can extract the calculated pressure as the derivative of the energy with respect to the volume and we find $P = 93$ GPa. This is much higher than the pressure at which the experimental XMCD signal disappears, $P = 28$ GPa. The calculations are performed at low temperature (0 K) so it is not surprising to find a transition pressure larger than the one measured at room temperature, but the main reason of this discrepancy is likely that the uncertainty on the calculated transition pressure is very large (several tens of GPa). This is due to the fact that a small error on the lattice parameter *a* results in a significant error

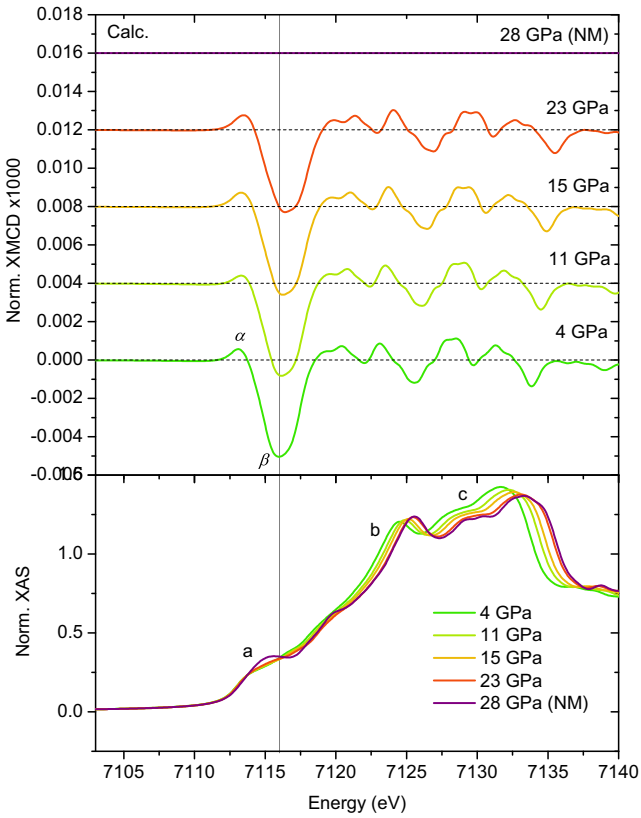

FIG. 8. Calculated XAS and XMCD spectra without core hole at the Fe *K* edge in FeH at several pressures. The calculation for 28 GPa is not spin polarized so that no XMCD can be computed.

on the volume and pressure varies quickly with volume in the range 40–45 $Å^3$ (the volume $V = 45\,Å^3$ corresponds to a pressure $P = 40$ GPa). Therefore, the crossing of the two curves in Fig. 7 allows us to assert the possibility of a magnetic transition under pressure but not to determine the transition pressure.6

The XAS and XMCD spectra without core hole [37] of the ferromagnetic state of dhcp-FeH were computed with several lattice parameters corresponding to pressures between 4 and 23 GPa. They are shown in Fig. 8. By comparison with Fig. 6, we see that our calculations reproduce very well the effect of pressure measured on the experimental spectra. The effect of pressure on the XAS spectra of ferromagnetic FeH is to push the peaks at higher energies as the distances are reduced: peak *c* is shifted by 1.5 eV between 4 and 23 GPa. The amplitude of XMCD decreases slowly without changing its shape. The maximum of the effect is slightly shifted to higher energies: peak β is shifted by 0.5 eV between 4 and 23 GPa. The fact that the full width at half maximum is kept constant (1.6 eV) over the whole energy range in the calculation allows us to obtain miscellaneous peaks at higher energies which are not visible in experiment. We observe that the peak in XMCD at 7132 eV (energy of peak *c*) is shifted by 1.5 eV between 4 and 23 GPa so that the shift in energy of the XMCD features is exactly the same as the shift of the XAS features.

Experimentally, the only change on the XAS spectrum between 4 and 23 GPa (see bottom panel of Fig. 6) is a progressive shift of the features to higher energies as the sample is compressed due to the reduction of distances: peak *c*, for example, is shifted by 1.6 eV between 4 and 23 GPa. The main effect of pressure on the XMCD spectrum (see top panel of Fig. 6) is a slight decrease in amplitude. The maximum of the effect is also progressively shifted to higher energies: peak β is shifted by 0.6 eV between 4 and 23 GPa.

The calculation for $P = 28$ GPa is for a nonmagnetic state (i.e., a state where all atoms have no net magnetic moments), hence the XMCD signal is exactly zero. The similarity between the calculated XAS spectra for the nonmagnetic state and the experimental XAS spectra at 28 GPa is striking: the shoulders *a* and *b* are enhanced while the maximum *c* decreases in amplitude. From this comparison, we can conclude that the evolution of the shape of the experimental XAS spectra at 28 GPa is a marker of the transition from ferromagnetic FeH to paramagnetic FeH that is not accompanied by any structural transition.

IV. CONCLUSION

By a combined experimental and theoretical approach, we have studied two transitions that occur when Fe is compressed under H_2 atmosphere.

The first transition corresponds to the absorption of H atoms into the bcc-Fe lattice which leads to the formation of dhcp-FeH. The calculated spectra for bcc-Fe and dhcp-FeH are in good agreement with experimental ones. This indicates that FeH is well simulated by our DFT-based numerical method, up to fine effects of the H atoms on the electronic structure of the Fe atoms. Indeed, we showed that the presence of H atoms have a notable effect on the XMCD spectra. This effect is stronger on one type of Fe atoms in the dhcp structure than on the other. We showed that the changes of XMCD signals are direct signatures of the variation of the spin-polarized electronic distribution that is much more sensitive than aggregate parameters such as the total magnetic moment.

The second transition is a purely magnetic transition from a ferromagnetic state to a paramagnetic state with no crystallographic transition. The existence of this pressure-induced transition, which was first inferred from the observation of the experimental XMCD spectra, was confirmed by the numerical calculations of the electronic states and by the computation of the XAS and XMCD spectra. These calculations have proven to be a useful tool to understand the changes of XAS spectra under pressure in the absence of a structural transition. This is not obvious when, as in the case presented here, pressure induces not only the expected stretch of the energies due to distances contraction, but also a variation of the intensities of the peaks.

ACKNOWLEDGMENTS

Interesting discussions with Christian Brouder are gratefully acknowledged. This work was supported by French state funds managed by the ANR within the Investissements d'Avenir programme under Ref. No. ANR-11-IDEX-0004-02, and more specifically within the framework of the Cluster of Excellence MATISSE led by Sorbonne Universités. The numerical calculations have been performed using HPC resources from GENCI-IDRIS (Grant No. 2017-100172).

[1] F. Birch, J. Geophys. Res. **57**, 227 (1952).
[2] K. Sakamaki, E. Takahashi, Y. Nakajima, Y. Nishihara, K. Funakoshi, T. Suzuki, and Y. Fukai, Phys. Earth Planet. Inter. **174**, 192 (2009).
[3] L. Schlapbach and A. Zuttel, Nature (London) **414**, 353 (2001).
[4] V. E. Antonov, I. T. Belash, E. G. Ponyatovskii, V. G. Thiessen, and V. I. Shiryaev, Phys. Status Solidi A **65**, K43 (1981).
[5] J. V. Badding, R. J. Hemley, and H. K. Mao, Science **253**, 421 (1991).
[6] G. van der Laan, I. Figueroa, Coord. Chem. Rev. **277-278**, 95 (2014).
[7] B. T. Thole, P. Carra, F. Sette, and G. van der Laan, Phys. Rev. Lett. **68**, 1943 (1992).
[8] P. Carra, B. T. Thole, M. Altarelli, and X. Wang, Phys. Rev. Lett. **70**, 694 (1993).
[9] M. Altarelli, Phys. Rev. B **47**, 597 (1993).
[10] N. Bouldi, N. J. Vollmers, C. G. Delpy-Laplanche, Y. Joly, A. Juhin, P. Sainctavit, C. Brouder, M. Calandra, L. Paulatto, F. Mauri *et al.*, Phys. Rev. B **96**, 085123 (2017).
[11] J. C. Chervin, B. Canny, J. M. Besson, and P. Pruzan, Rev. Sci. Instrum. **66**, 2595 (1995).
[12] A. P. Jephcoat, H. K. Mao, and P. M. Bell, J. Geophys. Res. Solid Earth **91**, 4677 (1986).
[13] F. Baudelet, Q. Kong, L. Nataf, J. D. Cafun, A. Congeduti, A. Monza, S. Chagnot, and J. P. Itié, High Press. Res. **31**, 136 (2011).
[14] P. Giannozzi *et al.*, J. Phys.: Condens. Matter **21**, 395502 (2009).
[15] M. Taillefumier, D. Cabaret, A.-M. Flank, and F. Mauri, Phys. Rev. B **66**, 195107 (2002).
[16] C. Gougoussis, M. Calandra, A. P. Seitsonen, and F. Mauri, Phys. Rev. B **80**, 075102 (2009).
[17] N. Troullier and J. L. Martins, Phys. Rev. B **43**, 1993 (1991).
[18] J. P. Perdew, K. Burke, and M. Ernzerhof, Phys. Rev. Lett. **77**, 3865 (1996).
[19] U. Gerstmann, N. J. Vollmers, A. Lücke, M. Babilon, and W. G. Schmidt, Phys. Rev. B **89**, 165431 (2014).
[20] N. Bouldi and C. Brouder, Eur. Phys. J. B **90**, 246 (2017).
[21] J. E. Müller, O. Jepsen, and J. W. Wilkins, Solid State Commun. **42**, 365 (1982).
[22] K. Momma and F. Izumi, J. Appl. Crystallogr. **44**, 1272 (2011).
[23] A. Kokalj, Comp. Mater. Sci. **28**, 155 (2003).
[24] C. Kittel, *Introduction to Solid State Physics*, 8th ed. (Wiley, New York, 2004), Chap. 1.
[25] V. E. Antonov, K. Cornell, V. K. Fedotov, A. I. Kolesnikov, E. G. Ponyatovsky, V. I. Shiryaev, and H. Wipf, J. Alloys Compd. **264**, 214 (1998).
[26] T. Tsumuraya, Y. Matsuura, T. Shishidou, and T. Oguchi, J. Phys. Soc. Jpn. **81**, 064707 (2012).
[27] P. Vinet, J. H. Rose, J. Ferrante, and J. R. Smith, J. Phys. Condens. Matter **1**, 1941 (1989).
[28] N. Ishimatsu, T. Shichijo, Y. Matsushima, H. Maruyama, N. Kawamura, M. Mizumaki, T. Matsuoka, and K. Takemura, J. Phys. Conf. Ser. **377**, 012041 (2012).
[29] I. Choe, R. Ingalls, J. M. Brown, Y. Sato-Sorensen, and R. Mills, Phys. Rev. B **44**, 1 (1991).
[30] G. Schneider, M. Baier, R. Wordel, F. Wagner, V. Antonov, E. Ponyatovsky, Y. Kopilovskii, and E. Makarov, J. Less-Common Met. **172**, 333 (1991).
[31] C. Elsässer, J. Zhu, S. G. Louie, B. Meyer, M. Fähnle, and C. T. Chan, J. Phys. Condens. Matter **10**, 5113 (1998).
[32] R. Torchio, O. Mathon, and S. Pascarelli, Coord. Chem. Rev. **277-278**, 80 (2014).
[33] T. Mitsui and N. Hirao, MRS Proc. **1262**, 1262-W06-09 (2010).
[34] C. M. Pépin, A. Dewaele, G. Geneste, P. Loubeyre, and M. Mezouar, Phys. Rev. Lett. **113**, 265504 (2014).
[35] S. Mankovsky, S. Polesya, H. Ebert, W. Bensch, O. Mathon, S. Pascarelli, and J. Minár, Phys. Rev. B **88**, 184108 (2013).
[36] F. D. Murnaghan, Proc. Natl. Acad. Sci. USA **30**, 244 (1944).
[37] Computation of the spectra without core hole requires much less computational resources than calculations with a core hole—because there is no need to use a supercell—and it does not prevent from studying the variation of the spectra with a given parameter (e.g., pressure).